Wave function mapping of graphene quantum dots with soft confinement

D. Subramaniam[1], F. Libisch[2], Y. Li[3], C. Pauly[1], V. Geringer[1], R. Reiter[2], T. Mashoff[1], M. Liebmann[1], J. Burgdörfer[2], C. Busse[4], T. Michely[4], R. Mazzarello[3], M. Pratzer[1],* and M. Morgenstern[1]

[1] *II. Physikalisches Institut B and JARA-FIT, RWTH Aachen University, D-52074 Aachen, Germany*

[2] *Institute for Theoretical Physics, Vienna University of Technology, A-1040 Vienna, Austria*

[3] *Institute for Theoretical Solid State Physics and JARA-FIT, RWTH Aachen University, D-52074 Aachen, Germany*

[4] *II. Physikalisches Institut, Universität zu Köln, Zülpicherstr. 77, D-50937 Köln, Germany*

(Dated: January 20, 2013)

Using low-temperature scanning tunneling spectroscopy, we map the local density of states (LDOS) of graphene quantum dots supported on Ir(111). Due to a band gap in the projected Ir band structure around the graphene K point, the electronic properties of the QDs are dominantly graphene-like. Indeed, we compare the results favorably with tight binding calculations on the honeycomb lattice based on parameters derived from density functional theory. We find that the interaction with the substrate near the edge of the island gradually opens a gap in the Dirac cone, which implies soft-wall confinement. Interestingly, this confinement results in highly symmetric wave functions. Further influences of the substrate are given by the known moiré potential and a 10 % penetration of an Ir surface resonance into the graphene layer.

PACS numbers: 73.20.At, 72.10.Fk, 73.21.Fg, 73.22.Pr

Graphene has moved in short time from first preparation as a small flake [1] towards possible applications such as high frequency transistors [2], supercapacitors [3] or touch screens [4]. Another exciting perspective is to use graphene quantum dots (QDs) as spin qubits [5]. The basic prerequisite is a very long spin coherence time [6], which might exist in graphene [7] due to the absence of hyperfine coupling in isotopically pure material and the small spin-orbit coupling [8]. First graphene QDs have been produced and probed by transport measurements [9, 10]. However, since graphene provides no natural gap, it is difficult to control the electron number [11]. Moreover, the 2D sublattice symmetry makes the QD properties very susceptible to the atomic edge configuration [5] unlike conventional QDs. As a result, chaotic Dirac billiards have been predicted [12] and were even claimed to be realized [9, 13], i.e. the wave functions are assumed to be rather disordered. To achieve improved control of graphene QDs, the QD edges must be well defined and a deeper understanding of the QD properties is mandatory.

Direct insight into QD properties is provided by scanning tunneling spectroscopy (STS) which maps out the squared wave functions of QDs [14] and, at the same time, determines the shape of the QD atom by atom. Using STS, we probe graphene QDs with well defined zigzag edges supported on an Ir(111) surface [15]. These QDs maintain graphene properties as the filled part of the graphene Dirac cone lies in the Ir projected band gap [16]. By comparing the measured wave functions with model calculations, we determine the relationship between geometry and electronic properties and extract general trends. Most notably, the soft edge potential provided by the interaction of the QD edges with the substrate enhances the geometrical symmetry of the wave functions, thus rendering the QD more regular. The susceptibility of the wave functions to the edge configuration is intimately related to the additional sublattice symmetry (pseudospin) which makes graphene so special [17]. Also the moiré pattern induced by the graphene-Ir lattice mismatch [16] and the hybridization of graphene with an Ir surface resonance are shown to have an influence on the measured wave functions.

STM measurements are performed in ultrahigh vacuum at $T = 5\,\mathrm{K}$ [18]. Monolayer graphene islands are prepared by exposing clean Ir(111) for 4 min to a pressure of 10^{-5} Pa of C_2H_4 at 300 K and subsequent annealing to 1320 K (30 s) [19]. The resulting graphene QDs have diameters of $2 - 40\,\mathrm{nm}$ as shown in Fig. 1a.

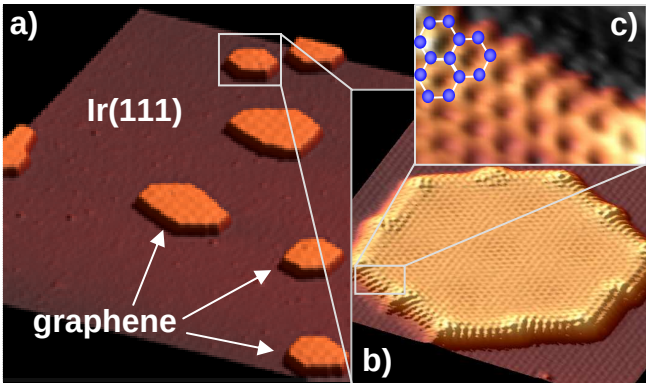

FIG. 1. (color online) (a) $(100 \times 100)\,\mathrm{nm}^2$ STM image of Ir(111) covered by monolayer graphene islands; $U = -0.3$ V, $I = 0.3\,\mathrm{nA}$; (b) atomically resolved $(12 \times 12)\,\mathrm{nm}^2$ image of graphene island; (c) magnified view of zigzag edge with graphene lattice overlaid; $U = 0.7$ V, $I = 20\,\mathrm{nA}$.

* pratzer@physik.rwth-aachen.de

Atomically resolved QD images (Fig. 1b−c) reveal the complete enclosure of the QDs by zigzag edges.

The local density of states (LDOS) of 15 islands is mapped by STS. We use a lock-in technique with modulation frequency $\nu = 1.4\,\mathrm{kHz}$ and amplitude $U_{\mathrm{mod}} = 10\,\mathrm{mV}$ resulting in an energy resolution $\delta E \approx \sqrt{(3.3 \cdot k_B T)^2 + (1.8 \cdot eU_{\mathrm{mod}})^2} = 18\,\mathrm{meV}$ [20]. For dI/dU curves, we stabilize the tip at sample voltage U_{stab} and current I_{stab}. Figure 2a shows a dI/dU curve laterally averaged over the hexagonal QD shown to the right. It displays three maxima below the Dirac point E_{D}, which is slightly above the Fermi level E_{F} [16]. Thus, the peaks belong to confined hole states. Fig.2b-d show dI/dU maps at the peak energies. For the first peak ($U = -0.26\,\mathrm{V}$), one maximum of the LDOS in the center of the island appears, a ring shaped structure is observed at $U = -0.42\,\mathrm{V}$, and, a maximum-minimum-maximum sequence from the center towards the rim with an additional star-shaped angular dependence is visible at $U = -0.63\,\mathrm{V}$. We checked that no other LDOS shapes are present at $-1.4eV \leq U \leq 0\,\mathrm{V}$. From the sequence of observed LDOS shapes we conclude that they represent confined states of the QD.

To model the QD states, we employ third-nearest neighbor tight binding (TB) calculations [21–23] using the atomic configuration of the QD found by STM,

$$H = \sum_{i,s} |\phi_{i,s}\rangle\, V_i\, \langle\phi_{i,s}| + \sum_{(i,j),s} \gamma_{(i,j)}\, |\phi_{i,s}\rangle\, \langle\phi_{j,s}| + h.c.. \quad (1)$$

The $\gamma_{(i,j)}$ are hopping amplitudes between sites i and j being $\gamma_{(i,j)} = (3.14, 0.042, 0.35)$ eV for the (first, second, third) nearest-neighbors [21]. The V_i represent local on-site potentials.

We first employed a spatially constant V_i within the islands, i.e. hard-wall-confinement. Regular, but also very irregular wave functions result, as shown in Fig. 2h and Fig. 3e-g. The irregular wave functions often display a large intensity at the rim of the QDs and illustrate the sensitivity of graphene QDs to details of the edge configuration [5, 12]. Such irregular shapes, however, were never found in the present STS experiments featuring about 50 different states [24].

This failure is related to the two experimental facts that (i) a graphene flake bends downward from $D = 3.4$ Å in the center of a QD to $D = 1.6$ Å at its rim [15, 26] and that (ii) the entire graphene flake features a moiré type corrugation leading to minigaps [16, 27, 28].

To incorporate effect (i) we determined the band structure of graphene by *ab initio* density functional theory (DFT) calculations [24, 25] for different graphene-Ir surface distances D. Upper and lower limits for D were set by the known distance between extended graphene layers and Ir(111), $D = 3.4$ Å [26] and the smallest distance found at the edge of a graphene island, $D = 1.6$ Å [15]. A proper description of Ir(111) surface states requires thick slabs which makes it unfeasible to use the large 10×10 supercell necessary to account for the graphene-Ir lattice mismatch. Therefore, a slightly compressed Ir lattice is

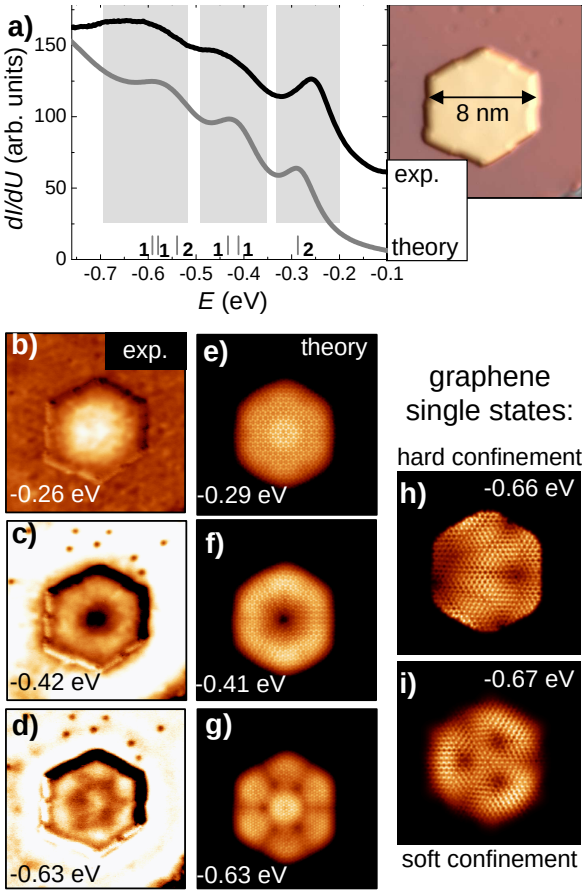

FIG. 2. (color online) (a) black line: $dI/dU(U)$ curve spatially averaged over the graphene QD shown to the right; $U_{\mathrm{stab}} = 0.5\,\mathrm{V}$, $I_{\mathrm{stab}} = 0.5\,\mathrm{nA}$, $U_{\mathrm{mod}} = 10\,\mathrm{mV}$; grey line: DOS(E) of the same island as obtained by TB calculation (see text); vertical bars mark the calculated eigenstate energies with degeneracies indicated as numbers; (b)-(d) dI/dU images recorded at energies $E = U \cdot e$ as marked; $I = 0.2\,\mathrm{nA}$; $U_{\mathrm{mod}} = 10\,\mathrm{mV}$. (e)-(g) LDOS maps calculated with soft edge potential at energies indicated; (h),(i): LDOS of an individual state calculated without (h) and with (i) soft edge potential.

used making graphene and Ir(111) commensurate. This allows us to work with a slab of 24 Ir layers with graphene on both sides and a vacuum space of 20 Å between slabs. The insets in Fig. 3a exhibit the resulting band structures for two different fixed D. The size of the gap ΔE_{D} is plotted in Fig. 3a. We incorporate the effect of the D dependent band-gap on V_i within the TB through [12]:

$$V_{i,\mathrm{rim}} = \Delta E[D(r_i)]/2 \cdot \sigma_z\,, \quad (2)$$

where the Pauli matrix σ_z acts on the sublattice degree of freedom. A homogeneous $V_{i,\mathrm{rim}}$ would open a gap of size ΔE at E_{D}. The functional form of $\Delta E[D] = (0.7 * (3.6 - D[\text{Å}])^2 + 0.23)$ eV is taken from the fit to the DFT calculations (Fig. 3a). We model the global height variation of a graphene QD by linear increase of $D(r)$ from the rim towards 10 Å inside the island as suggested by the DFT calculations of [15]. We checked that reason-

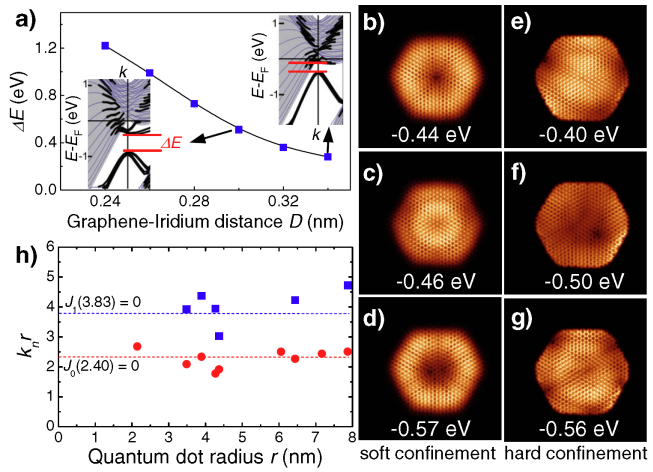

FIG. 3. (color online) (a) Energy gap ΔE versus graphene-Ir distance D as deduced from DFT calculations; insets: band structure around E_D for two different D as marked by arrows with ΔE indicated; grey area: projected bulk bands of Ir; Thick black lines: graphene states; (b)-(g) Calculated LDOS ($= |\Psi|^2$) for individual confined states with energies marked: (b)-(d) with soft edge potential; (e)-(g) without soft edge potential; (h) experimental $k_n \cdot r = E_n/(\hbar v_D) \cdot r$ for the two peaks closest to E_D at different average island radius r; circles: $n = 0$, squares: $n = 1$; dotted lines: zeros of the first two Bessel functions (see text).

able modifications do not change the results significantly [24].

To incorporate effect (ii), we added a moiré potential $V_{i,\mathrm{m}}$ to V_i. Based on the experimentally observed minigap of 200 meV [16, 27, 28], we use a harmonic variation of $V_{i,\mathrm{m}}$ in each of the three dense packed directions of graphene with a total amplitude of 400 meV [24]. Finally, the peak width Γ of the eigenstates is adapted to the experiment leading to $\Gamma(E) = 0.33 \cdot |E|$.

The resulting LDOS curve (grey line, Fig. 2a) as well as the calculated LDOS maps (Fig. 2e-g) exhibit excellent agreement with the experimental data. Importantly, the calculations yield only states that reflect the hexagonal symmetry of the QD shape in agreement with experiment, but none of the irregular states found without smooth confinement [24]. This can be rationalized by the suppressed interaction of the confined states with the zigzag edges, which would break sublattice symmetry [29]. The increased geometrical symmetry is illustrated in Fig. 3b-g comparing wave functions of the same quantum dot with soft (hard) confinement leading to symmetric (irregular) states. Thus, softly opening a band gap at the QD edge leads to strongly improved control on the states residing in its interior.

To illustrate this crucial finding, we show that the state energies in our QDs can be correctly estimated by a simplified circular flake geometry. We obtain $E_n = \hbar v_D k_n$ with Dirac velocity $v_D = 10^6$ m/s and k_n deduced from the Bessel functions:

$$J_n(k_n \cdot r) = 0, \quad n = 0, 1, ... \tag{3}$$

Up to an island area of $A = 150$ nm^2 (average radius: $r = \sqrt{A/\pi}$), the estimate fits the experimental peak energies to within $\sim$ 20 % for the two lowest energy states (Fig. 3h). Larger islands do not follow this trend because of their strong deviation from a circular shape (e.g. Fig. 4a). Obviously, neither the sensitive sublattice symmetry of graphene [5], nor the influence of the iridium substrate enter Eq. (3) showing the simplicity of softly confined graphene QDs. Note, in addition, that the agreement in Fig. 3h only uses the peak energies as an experimental reference and does not refer to the measured LDOS shapes. Thus, peak energies are compatible with $v_D = 1 \pm 0.1 \cdot 10^6$ m/s.

In larger islands, we observe the influence of $V_{i,\mathrm{m}}$ on wave function patterns directly, at energies $E < -0.6$ eV. Figure 4a shows an STM topography of a large QD exhibiting a regular moiré pattern [19]. The dI/dU map in Fig. 4b and the calculated LDOS in Fig. 4c reproduce the moiré topography albeit with inverted amplitude. The same result is found for all larger islands [24]. We checked that normalizing the dI/dU images to account for a spatially varying tip-surface distance [30] did not change the LDOS patterns.

One feature, already visible by comparing Fig. 4b and c, is not accounted for by a spatially varying V_i: a bright rim of the island in the dI/dU image. This rim is found for all islands, but cannot be reproduced by the TB calculations [24]. Closer to E_D, this feature develops into a standing wave pattern that finds its counterpart outside the island with slightly larger wave length λ (Fig. 4d–f). The dispersion relations $E(\Delta k = \pi/\lambda)$ [31] inside and outside the islands are evaluated as displayed in Fig. 4e and in [24] for 11 islands. They are shown together with results from standing waves at step edges of Ir(111) in Fig. 4g. The $E(\Delta k)$ curves are linear according to $E = -\hbar v_D \Delta k + E_D$ with $v_D \simeq 4.9 \cdot 10^5$ m/s, $E_D = -0.3$ eV outside the island and $v_D \simeq 4.5 \cdot 10^5$ m/s, $E_D = -0.2$ eV inside the island. These values agree with those of the Ir surface resonance S_0 around $\bar{\Gamma}$ found by photoemission (dashed line) including the energy offset between the two $E(\Delta k)$ curves [28]. The values disagree with v_D for the graphene Dirac cone on Ir(111) by a factor of two and with E_D for the Ir S2 surface state by 0.5 eV [16]. Thus, the standing wave patterns within the QD are attributed to an intrusion of S_0 into graphene. The amplitude of the standing wave in the islands A_G is found to be close to the amplitude outside the island A_{Ir} for several islands and energies [24]. This is surprising considering the fact that the tip is 0.23 nm further away from the Ir surface, when positioned above graphene, which would suggest a reduction in dI/dU intensity by a factor of 100 [20]. However, DFT calculations reveal that S_0, exhibiting sp-symmetry, penetrates into graphene. The ratio between the LDOS in the graphene layer I_C and the LDOS in the Ir surface layer I_{Ir} is $R_{DFT} = I_C/I_{Ir} \simeq 8 - 12$ % (inset of Fig. 4h).

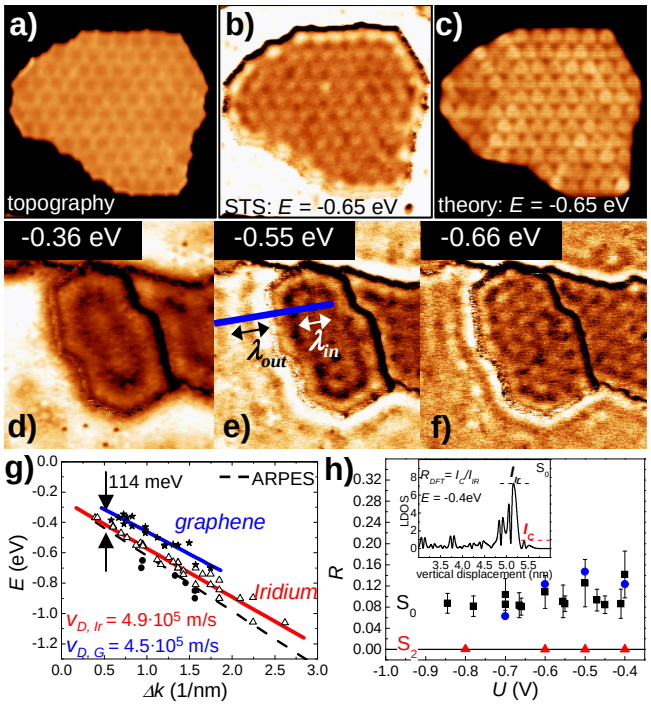

FIG. 4. (color online) (a) STM image and (b) dI/dU map of a large graphene QD; 30×30 nm^2, $U = -0.65$ V, $I = 0.5$ nA, $U_{\rm mod} = 10$ mV; (c) calculated LDOS of the same QD at $E = -0.65$ eV; (d)-(f) dI/dU maps of a graphene QD recorded at the energies marked; 27×30 nm^2, $I = 0.5$ nA, $U_{\rm mod} = 10$ mV; deduced wave lengths $\lambda_{\rm out}$ ($\lambda_{\rm in}$) outside (inside) the QD are marked in (e); (g) resulting dispersion relations $E(\Delta k = \pi/\lambda_{\rm in/out})$ inside (stars) and outside (triangles) of the QD as well as from standing waves scattered at Ir(111) step edges (circles); full lines are linear fits with resulting $v_{\rm D}$ indicated; energy offset is marked; dashed line is deduced from photoemission on clean Ir(111) [28]; (h) relative intensity R of S_0 and S_2 in graphene as deduced from STS data (squares) and from DFT calculations (S_0: circles, S_2: triangles); inset: calculated LDOS of S_0 at $E = -0.4$ eV along the direction perpendicular to the surface; $I_{\rm Ir}$ and $I_{\rm C}$ as used for determination of R are marked.

For comparison, S_2 shows only $R_{\rm DFT} \simeq 0.02$ %. Figure 4h favorably compares $R_{\rm DFT}$ of S_0 with the data from STS $R_{\rm STS}$ where the apparent $A_{\rm G}/A_{\rm Ir}$ is rescaled according to $R_{\rm STS} = A_{\rm G}/A_{\rm Ir} \cdot e^{\alpha\delta}$ [20] with $\alpha = 1.1 - 1.2$/Å deduced from $I(z)$ curves and $\delta = 1.1$ Å being the difference between real height (3.4 Å [26]) and apparent STM height (2.3 Å) of the graphene above the Ir(111). Thus, we can quantitatively reproduce the strength of S_0 intrusion into graphene. A simple explanation for the strong S_0 intrusion is not obvious, but we note that, according to DFT, also the d_z^2-like surface state S_1, located at E_F and exhibiting no dispersion [16], penetrates into graphene with $R \simeq 10 - 40$ % and the π-electrons of graphene penetrate back into Ir with $R \simeq 1 - 4$ %.

Finally, we would like to comment on the fact that the S_0 state partly dominates the LDOS patterns, while the peak energies are reproduced nicely by the Dirac cone of graphene. We assume that the life time of the graphene states is large enough to lead to confinement resonances appearing as peaks, while the life time of the S_0 is significantly shorter leading only to exponentially decaying standing waves at the step edges of the graphene islands. Indeed, we do not observe peaks within the spectroscopy of the islands, where the standing wave of S_0 is dominating the LDOS pattern. Moreover, the standing wave gets always significantly weaker in intensity away from the step edge. Of course, S_0 probably influences the LDOS patterns of the small islands as well, which might explain the remaining deviations between theory and experiment in Fig. 2 (e.g. (d) and (g)). This subtle interplay between graphene electrons and S_0 electrons within the graphene island might also explain the too low $v_{\rm D} = 6{\cdot}10^5$ m/s resulting from the analysis of the LDOS pattern of graphene quantum dot states on Ir(111) in ref. [32].

In conclusion, we mapped the LDOS of graphene QDs supported on Ir(111). For small islands, properties of an isolated graphene QD with soft edge potential reproduce the measured wave functions. Most importantly, the soft edge induced by the substrate is required for the experimentally observed high symmetry of the wave functions. Larger islands show an additional standing wave pattern caused by an intruding Ir surface resonance and signatures of the moiré potential.

We acknowledge helpful discussions with N. Atodiresei, C. Stampfer, G. Burkard, S. Runte, and a referee, as well as financial support by DFG (LI 1050/2-1, MO 858/8-2, BU 2197/2-1), Fonds National de la Recherche (Luxembourg), and FWF (SFB-F41 VICOM). Numerical calculations are performed on the Vienna Scientific Cluster (VSC)

Note added in proof: During the referee process, two publications with similar experimental results have been published [32], which were submitted later than our manuscript.

[1] K. S. Novoselov *et al.*, Science **306**, 666 (2004).
[2] Y. M. Lin*et al.*, Science **322**, 1294 (2011); **327**, 662 (2010); Y. Q. Wu *et al.*, Nature **472**, (2011).
[3] Y. Zhu *et al.*, Science **332**, 1537 (2011).
[4] K. S. Kim*et al.*, Nature **457**, 706 (2009).
[5] B. Trauzettel *et al.*, Nature Phys. **3**, 192, (2007); S. Das Sarma *et al.*, Rev. Mod. Phys. **83**, 407 (2011)
[6] D. Loss *et al.*, Phys. Rev A **57**, 120 (1998); C. H. Bennet *et al.* Nature *404*, 247 (2000).
[7] P. Struck *et al.*, Phys. Rev. B **82**, 125401 (2010).
[8] M. Gmitra *et al.*, Phys. Rev. B **80**, 235431 (2009); A. H. Castro-Neto et al., Phys. Rev. Lett. **103**, 026804 (2009).
[9] L. A. Ponamarenko *et al.*, Science **320**, 356 (2008).
[10] C. Stampfer *et al.*, Appl. Phys. Lett. **92**, 012102 (2008);

F. Molitor *et al.*, Appl. Phys. Lett. **94**, 222107 (2009); J. Güttinger *et al.*, Appl. Phys. Lett. **93**, 212102 (2008).
[11] J. Güttinger *et al.*, Phys. Rev. Lett. **103**, 046810 (2009); S. Neubeck *et al.*, Small **6**, 1469 (2010).
[12] M. V. Berry and R. J. Mondragon, Proceedings of the Royal Society of London, A **412**, 53-74 (1987).
[13] J. Wurm *et al.*, Phys. Rev. Lett. **102**, 056856 (2009), F. Libisch *et al.*, Phys. Rev. B **79**, 115423 (2009).
[14] J. T. Li *et al.*, Phys. Rev. Lett. **80**, 3332 (1998); T. Maltezopoulos *et al.*, Phys. Rev. Lett. **91**, 196804 (2003).
[15] P. Lacovig, *et al.*, Phys. Rev. Lett. **103**, 166101 (2009).
[16] I. Pletikosić *et al.*, Phys. Rev. Lett. **102**, 056808 (2009).
[17] K. S. Novoselov, A. K. Geim, Nature Mat. **6**, 183 (2007); A. H. Castro Neto *et al.*, Rev. Mod. Phys. **81**, 109 (2009); C. Lee *et al.*, Science **312**, 385 (2008).
[18] T. Mashoff, M. Pratzer, M. Morgenstern, Rev. Sci. Instrum. **80**, 053702 (2009).
[19] A. T. N'Diyae *et al.*, New. J. Phys. **10**, 043033 (2008); Phys. Rev. Lett. **95**, 215501 (2006).
[20] M. Morgenstern, Surf. Rev. Lett. **10**, 933 (2003).
[21] S. Reich *et al.*, Phys. Rev. B **66**, 035412 (2002).
[22] A. Grüneis *et al.* , Phys. Rev. B **78**, 205425 (2008).
[23] F. Libisch *et al.* , Phys. Rev. B, **81**, 245411 (2010).
[24] see supplemental material at ...
[25] P. Giannozzi *et* al., J. Phys.: Condens. Matter 21, 395502 (2009), http://www.quantum-espresso.org.
[26] C. Busse *et al.*, Phys. Rev. Lett. **107**, 036101 (2011).
[27] S. Rusponi *et al.*, Phys. Rev. Lett. **105**, 246803 (2010).
[28] A. Varykhalov *et al.*, ArXiv 1104.3308; J. v.d Veen *et al.*, Phys. Rev. B **22**, 4226 (1980).
[29] K. Nakada *et al.*, Phys. Rev. B **54**, 17954 (1996).
[30] C. Wittneven *et al.*, Phys. Rev. Lett. **81**, 5616 (1998).
[31] Plotting $E(\pi/\lambda)$ for standing waves would correspond to plotting the usual $E(2\pi/\lambda)$ for Bloch waves; E. J. Heller *et al.*, Nature **369**, 464 (1994).
[32] S. H. Park *et al.*, ACS Nano **5**, 8162 (2011); S. K. Hämäläinen *et al.*, Phys. Rev. Lett **107** 236803 (2011).

Supplementary information: Wave function mapping in graphene quantum dots

D. Subramaniam[1], F. Libisch[2], C. Pauly[1], V. Geringer[1], T. Mashoff[1], M. Liebmann[1], R. Reiter[2], Y. Li[3], J. Burgdörfer[2], C. Busse[4], T. Michely[4], R. Mazzarello[3], M. Pratzer[1],* and M. Morgenstern[1]

[1]*II. Physikalisches Institut B and JARA-FIT, RWTH Aachen University, D-52074 Aachen, Germany*

[2] *Institute for Theoretical Physics, Vienna University of Technology, A-1040 Vienna, Austria*

[3]*Institute for Theoretical Solid State Physics and JARA-FIT, RWTH Aachen University, D-52074 Aachen, Germany*

[4]*II. Physikalisches Institut, Universität zu Köln, Zülpicherstr. 77, D-50937 Köln, Germany*

(Dated: January 20, 2013)

* pratzer@physik.rwth-aachen.de

I. IMAGE GALLERY OF INVESTIGATED QUANTUM DOTS

Figure 1 shows an STM image gallery of all investigated graphene quantum dots (QDs) on the Ir(111) substrate. Detailed comparisons of dI/dU images and dI/dU curves with the results from third nearest neighbor tight binding calculations have been performed for theses islands, but only representative data are shown.

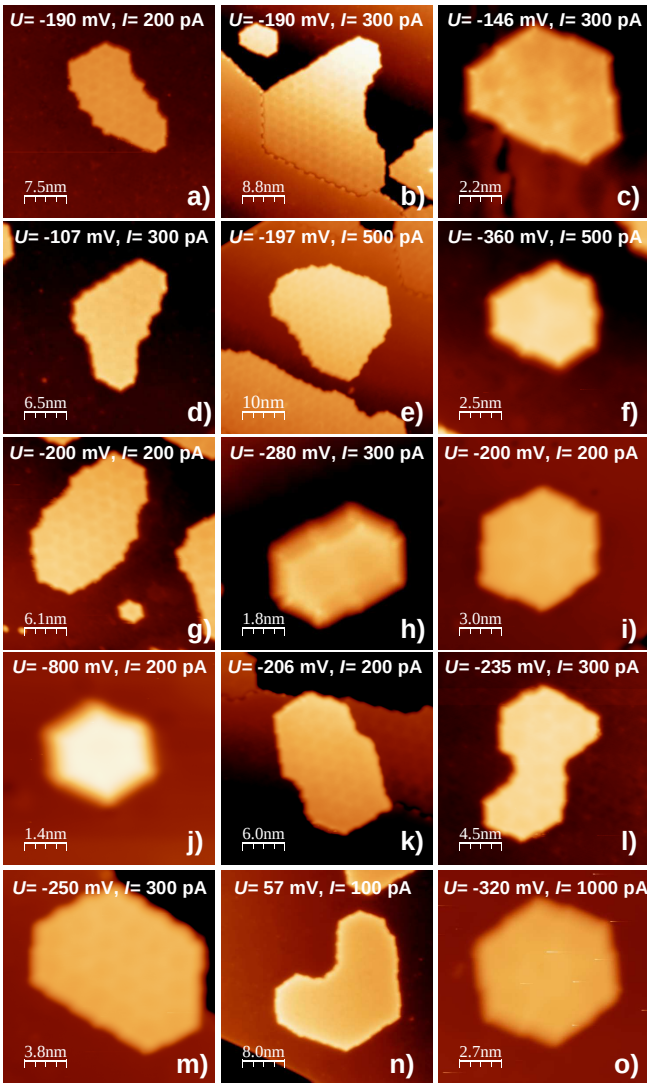

FIG. 1. Constant current STM images of investigated graphene QDs. Tunneling parameters are marked in the images.

II. DENSITY FUNCTIONAL THEORY (DFT) CALCULATIONS

Ab initio DFT simulations were carried out using the plane-wave PWSCF code included in the QUANTUM-ESPRESSO package [1].

We firstly studied the relationship between the size of the band gap in graphene and the graphene-Ir surface distance D, ranging from $D = 3.4$ Å to $D = 1.6$ Å. A 1×1 cell with the graphene cell parameter was used, which corresponds to a slightly compressed Ir(111) surface. We use a slab of 24 Ir layers with graphene on both sides and a vacuum space of 20 Å between slabs. We employed gradient-corrected exchange correlation functionals [2] and fully-relativistic ultrasoft pseudopotentials including spin-orbit interactions [3]. The wave functions were expanded in plane waves with a kinetic energy cutoff of 30 Ry and a charge-density cutoff of 300 Ry. $20 \times 20 \times 1$ Monkhorst-Pack meshes [4] of k-points were used for the integration over the Brillouin zone.

The electronic band structure of the system was computed along the $\bar{T}$, $\bar{T}'$ and $\bar{\Sigma}$ lines of the surface Brillouin zone, corresponding to the path $\bar{\Gamma} - \bar{K} - \bar{M} - \bar{\Gamma}$ in the reciprocal space. The graphene states were identified by projecting the wavefunctions of the slab on the atomic wavefunctions centered on the C atoms with a threshold of 50 %. This allowed us to calculate the gap ΔE between the lower and upper graphene cone as a function of the graphene-Ir distance (see main text). The absolute value of the Dirac point energy with respect to the Fermi level E_{F} at equilibrium distance ($D = 3.4$ Å) slightly deviates (by 200 meV) from photoemission experiments [5]. The band gap has also been estimated from the photoemission data to be 100 meV [5], i.e. 100 meV smaller that the one found by DFT at the equilibrium distance. We assume that these discrepancies are caused by the compression of the Ir(111) within the DFT calculations, but does not affect the general trend of increasing the band gap with shortened graphene-Ir distance.

Very recently, Varykhalov *et. al.* [6] detected a large Rashba effect on a surface state of Ir(111) (denoted as S_0 in the main text) near the $\bar{\Gamma}$ point: the properties of this state were found to be hardly affected when the surface is covered with graphene. We accordingly carried out DFT simulations of both the clean Ir(111) surface with a lattice constant of $a_0 = 2.758$ Å, corresponding to the value of $a_{fcc} = 3.90$ Å for bulk fcc Ir obtained from DFT calculations, and the graphene-Ir system with $D = 3.4$ Å. For these calculations, we also used a 24-layer Ir slab and identified the Ir(111) surface states by projecting them

onto the atomic orbitals of the surface and subsurface Ir atoms requiring more than 25 % of their weight located at these atoms. We found the surface state S_0, which is rather a surface resonance, in both cases. The band structure of the graphene-Ir system along the $\bar{\Gamma} - \bar{M}$ direction is shown in Fig. 2 with the surface resonance marked. The penetration of the surface resonance S_0 (as well as of the surface state S_2) into the graphene layer was calculated by relating the weight on the C atoms I_C to the weight on the Ir surface atoms I_{Ir} using $R_{DFT} = I_C/I_{Ir}$ (see main text).

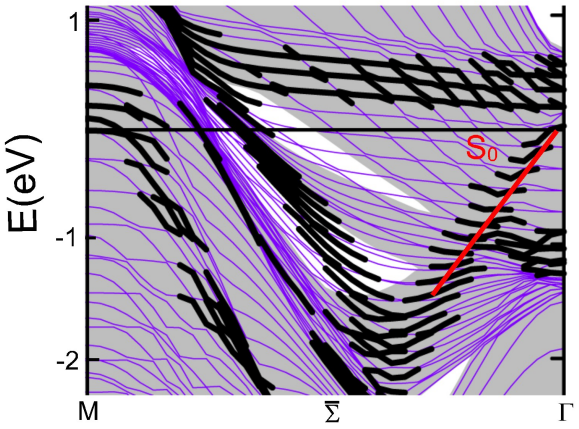

FIG. 2. Band structure of the graphene-Ir system along the $\bar{\Gamma} - \bar{M}$ direction. The dispersion of the S_0 surface resonance is indicated by a red line. The state has been identified by requiring that the sum of the squares of the projections of the state on the orbitals of the atoms of the surface and subsurface layer be larger than 0.25.

III. CONFINED POTENTIAL USED FOR THE CALCULATION

The potential V_i used for the tight binding calculation is modeled according to the distance D from the graphene sheet to the Ir surface [see Eq. (2) in main text]. We use a Berry-Mondragon like potential $V_i = \Delta E[D]/2 \cdot \sigma_z$ to model the gap opening at the Dirac point, as taken from our DFT calculations (see Fig.3a of main text). Consequently, the potential conserves K-K' symmetry [7] and models the (partial) hybridization of the carbon p_z orbitals with the Ir states known from our DFT calculations. Since the graphene quantum dot approaches the Ir surface at the edges, we obtain a smooth edge confinement that is key to

the formation of states with high symmetry observed in the experimental LDOS patterns. Near the edges, we assume a linear approach (as the most simple model) of the graphene sheet towards the Ir substrate from the equilibrium distance of 3.4 Å to 1.6 Å at the edge over a distance of 10 Å. To assert that this choice does not influence our conclusions, we have performed calculations for several different functional forms for distance between the quantum dot and the Iridium surface keeping the outmost distance of 1.6 Å fixed. Excluding unphysical, vertical kinks in the shape of the graphene flake, we find no noticeable changes in the wavefunction patterns (see Fig. 3). The variations in calculated resonance energies for different types of edge potentials are below 15 meV, which is smaller than the experimental energy resolution.

Secondly, the lattice mismatch between Ir and graphene is taken into account by a spatially varying moiré potential $V_{\mathrm{m}}(x, y)$, which consists of a suitable superposition of sinusoidal functions in accordance with ref. [8, 9] (see main text). In order to obtain the amplitude V_{max} of V_{m}, we perform tight binding calculations of the bandstructure of an infinitely extended graphene sheet in the presence of V_{m} for different V_{max}, and extract the size of the minigap Δ induced by zone folding [5]. Comparing to ARPES measurements, which feature $\Delta \simeq 200$ meV [5], we obtain $V_{\mathrm{max}} = 400$ meV.

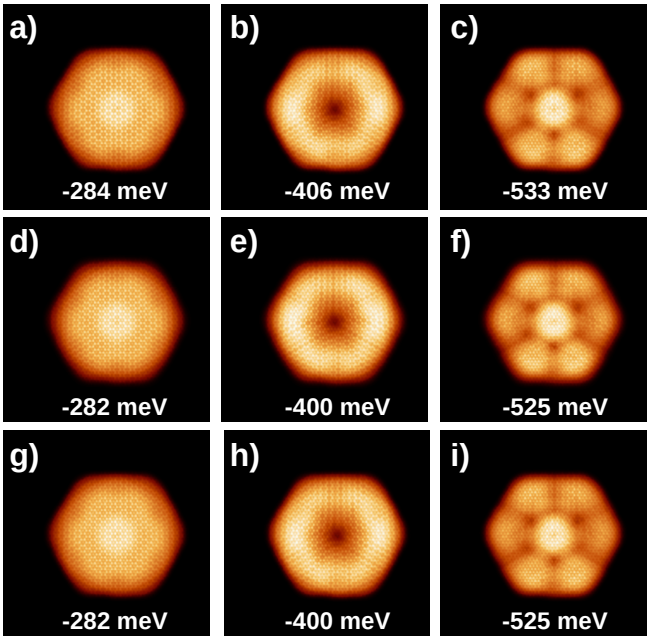

FIG. 3. The three lowest-lying eigenstates with their eigenenergies marked for different parametrizations of the distance development between the graphene quantum dot and the iridium substrate at the edge of the quantum dot: (a)-(c) linear interpolation $\propto x$ over 15 Å, i.e. $D(r_\perp) = 3.4 - 0.12 \cdot (15 - r_\perp) \cdot \theta(15 - r_\perp)$ with $r_\perp$, D in Å and $\theta(x)$ being the step function; (d)-(f) $x^{3/2}$ over 10 Å, i.e. $D(r_\perp) = 3.4 - 0.057 \cdot (10 - r_\perp)^{3/2}\theta \cdot (10 - r_\perp)$; (g)-(i) quadratic interpolation ($\propto x^2$) over 10 Å, i.e. $D(r_\perp) = 3.4 - 0.018 \cdot (10 - r_\perp)^2 \cdot \theta(10 - r_\perp)$; in the main manuscript, a linear interpolation over 10 Å was used (see main manuscript, Fig. 2).

IV. CALCULATED STATES WITHOUT SOFT EDGE POTENTIAL

Figure 4i shows an STM image of a particular island with the corresponding dI/dU maps displayed in Fig. 4 e−h. We display all patterns of dI/dU maps found in the voltage range between $U = -0.2$ V and $U = -0.6$ V. For comparison, wave functions are calculated by the third nearest neighbor tight-binding calculation neglecting the soft edge, i.e. $V_i = \infty$ outside the island. Inside the island, the moiré potential is maintained. Superpositions of squared wave functions at the energies corresponding to the dI/dU images are shown in Fig. 4 a−d. Only the two very similar states belonging to K and K' are superposed in Fig. 4a−c. In Figure 4d already 6 states, which have a very similar energy, had to be superposed. The shapes of the wave functions and the LDOS correspond to the measured dI/dU maps and the energies reasonably well, but the calculated shapes are less regular and more extended

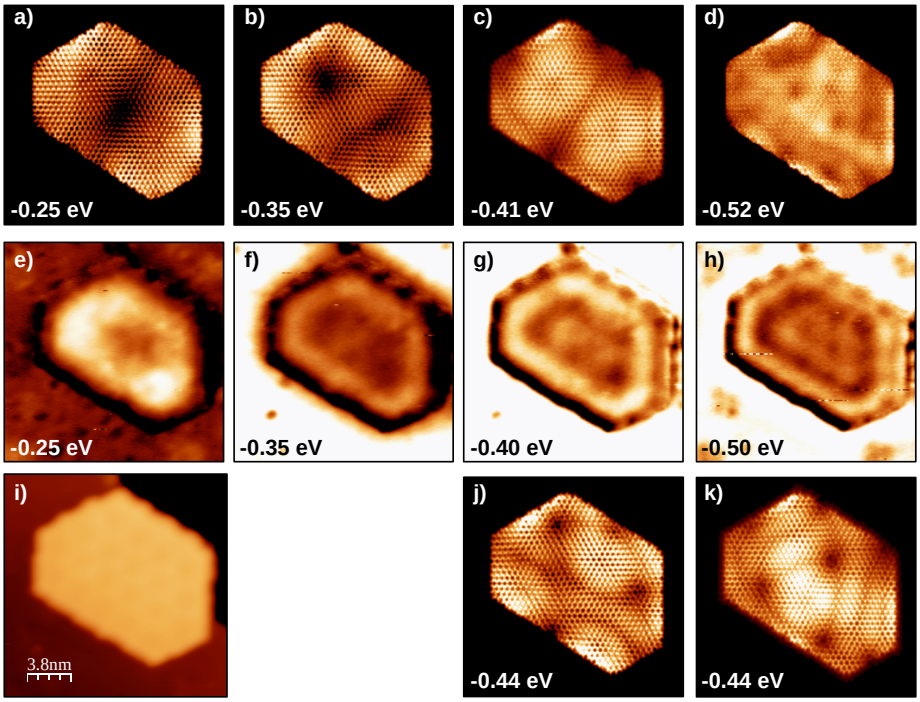

FIG. 4. (a)-(c) calculated squared wave functions of the island shown in (i) at energies marked; (d) calculated LDOS of the same island (consisting of 6 wave functions) at the energy marked; (e)-(h) dI/dU maps of the island shown in (i) at different energies $E = U \cdot e$ as marked; $I = 0.3$ nA, $U_{\mathrm{mod}} = 10$ mV; (i) STM image of the graphene QD; $U = -250$ mV, $I = 0.3$ nA; (j)-(k) calculated squared wave functions of the QD shown in (i) not found in experiment; all calculations are with abrupt edge.

towards the edge. Moreover, the calculated wave functions displayed in Fig. 4 j−k do not resemble the experimental LDOS maps. These wave functions feature a strong weight at the edge of the QD. They are suppressed by the soft confinement caused by hybridization of the graphene p_z orbitals with the iridium substrate.

V. STATES DOMINATED BY THE MOIRÉ POTENTIAL

For energies below -0.6 eV, the dI/dU maps are dominated by the moiré potential (see, e.g., the three islands in Fig. 5). The experimental data (left images) correspond to the calculated LDOS maps (right images) being prone to the moiré potential with amplitude 400 meV. Neglecting this moiré potential leads to more uniform wave patterns in the LDOS maps (not shown). Notice that a bright rim is visible in all experimental LDOS maps of Fig. 5 as well as in Fig. 4(f)-(h), which is not reproduced by the calculation and attributed to the Ir surface resonance around $\overline{\Gamma}$ (see main text).

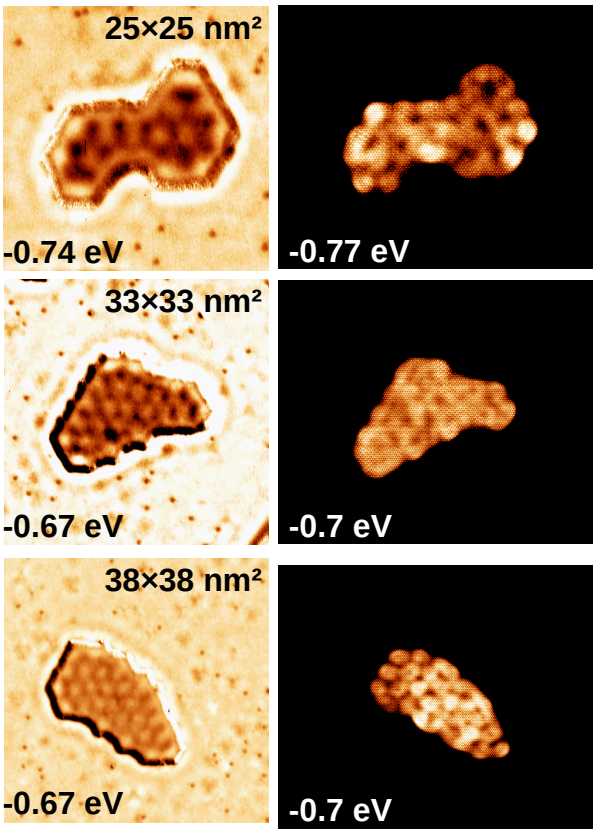

FIG. 5. dI/dU maps (left images) of different graphene QDs imaged at energies below -0.6 eV ($I = 0.4$ nA, $U_{\mathrm{mod}} = 10$ mV). The images are dominated by the moiré potential and are largely reproduced by the calculation (right images).

VI. STANDING WAVES OUTSIDE THE GRAPHENE ISLAND

Figure 6 shows dI/dU maps of three different quantum dots where the contrast is tuned in order to see the standing wave outside the QD. Obviously the wavelengths of these standing waves $\lambda_{\rm out}$ is decreasing with decreasing energy. By line scans, as shown in Fig. 6m for the dI/dU map in Fig. 6j, we deduced the $E(\pi/\lambda_{\rm out})$ dispersion shown in Fig. 4g of the main text. Since the measured standing wave pattern exhibits half the wave length of the impinging Bloch wave, $\Delta k = \pi/\lambda_{\rm out}$ is used such that the dispersion $E(\Delta k)$ can directly be compared with data from angular resolved photoelectron spectroscopy (ARPES) [6].

The standing waves are also observed at step edges of the Iridium(111) surface not covered by graphene. Figure 7a shows an STM image of the uncovered Ir(111) surface with two step edges. The two white dots are larger adsorbates on the surface. The dI/dU images exhibit standing waves at the step edges whose wave length decreases with decreasing energy. In addition, remaining oxygen adsorbates on the surface are visible as black dots which induce an additional complicated scattering pattern on the terraces. The wave lengths $\lambda_{\rm Ir}$ of the standing waves at the step edges are determined by line scans averaging along the step edge and the resulting $E(\pi/\lambda_{\rm Ir})$ is also plotted in Fig. 4g of the main text. The symbols in Fig. 4g of the main text exhibit a very similar steepness of $E(\pi/\lambda_x)$ ($x = {\rm in}, {\rm out}, {\rm Ir}$) for all three measurements, but the absolute values are lowest for the pure Ir(111) surface, slightly higher (about 50 meV) for the standing waves around the graphene QDs and the highest for the standing waves inside the graphene QDs being another 100 meV higher. The photoemission data [6] show the same energy shift of the dispersion of the state S_0 by about 150 meV between uncovered Ir(111) and Ir(111) completely covered with graphene.

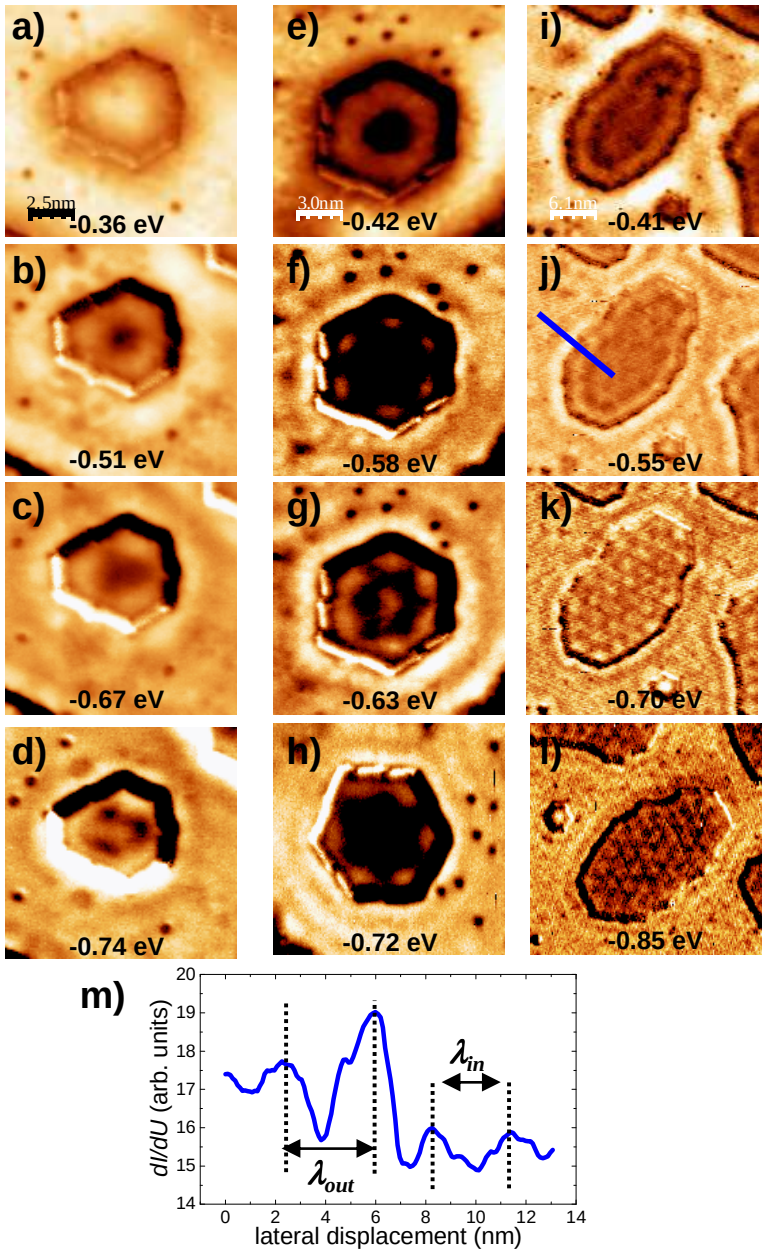

FIG. 6. (a)-(l) dI/dU maps of three different graphene QDs recorded at the energies $E = U \cdot e$ marked; $U_{\mathrm{mod}} = 10$ mV; (a)-(d),(i)-(l) $I = 0.2$ nA, (e)-(h) $I = 0.5$ nA; all images exhibit a standing wave around the island; wave length decreases with decreasing energy; blue line in (j) marks the line for the line scan shown in (m); (m) line scan along the line shown in (j); the deduced wave lengths of the standing waves inside (λ_{in}) and outside (λ_{out}) the QD are marked.

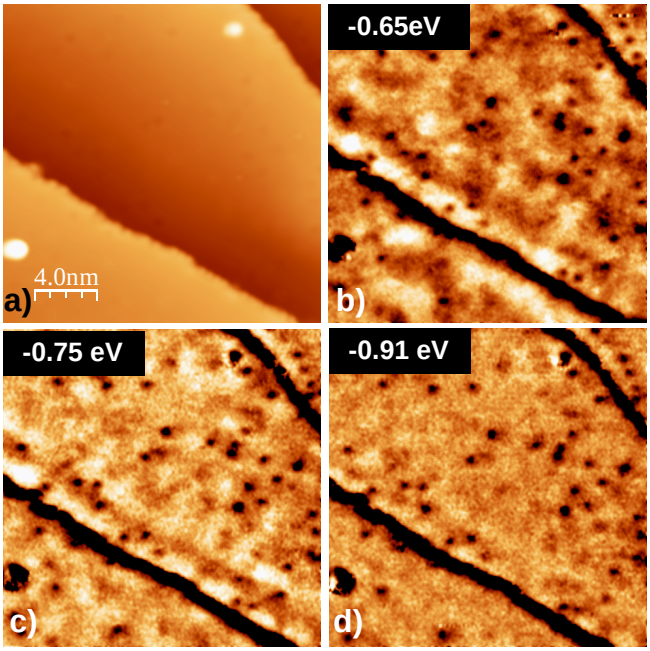

FIG. 7. (a) STM image of the Ir(111) surface with two step edges; $U = -0.2$ V; $I = 0.3$ nA; (b)-(d) dI/dU maps of the same area recorded at the energies $E = U \cdot e$ marked ($I = 0.3\,\mathrm{nA}$, $U_{\mathrm{mod}} = 10$ mV); standing waves are visible at the upper and the lower side of the step edges.

VII. ESTIMATE OF CONFINED ENERGIES

As described in the main text, we estimate the energy of confined states by the zeros of the first two Bessel functions according to:

$$J_n(k_n \cdot r) = 0, \quad n = 0, 1. \tag{1}$$

with eigenenergies $E_n = \hbar v_D k_n$, a Dirac velocity of graphene $v_D = 1 \cdot 10^6$ m/s and Radius r of the island. The first two peak energies E_0 and E_1 of the experiment are determined with respect to the Dirac point E_D for different islands. Since the shapes of larger islands become more irregular (see Fig. 1), only the nine smallest islands are considered. The average island radius r is deduced from the island area A by $r = \sqrt{A/\pi}$. The resulting $k_n \cdot r$ is plotted as a function of r for the two peak energies closest to E_D in Fig. 3 (h) of the main text. For a few of the islands, the energy of the 2$^{\mathrm{nd}}$ resonance in the dI/dU curve is not well defined due to broadening of lineshapes by finite state lifetime, and thus not considered in the present analysis. For the smallest island, only the first resonance energy lies within the Ir projected band gap. Obviously, reasonable agreement of the model with the experiment is found. The

discrepancy increases with radius which is attributed to the more non-circular shape of the larger islands.

---

[1] P. Giannozzi *et* al., J. Phys.: Condens. Matter 21, 395502 (2009), http://www.quantum-espresso.org.

[2] J. P. Perdew, K. Burke, and M. Ernzerhof, Phys. Rev. Lett. **77**, 3865 (1996).

[3] A. Dal Corso and A. Mosca Conte, Phys. Rev. B **71**, 115106 (2005).

[4] J. Monkhorst and J. D. Pack, Phys. Rev. B **13**, 5188 (1976).

[5] I. Pletikosić *et al.*, Phys. Rev. Lett. **102**, 056808 (2009); E. Starodub *et al.*, Phys. Rev. B **83**, 125428 (2011); S. Rusponi *et al.*, Phys. Rev. Lett. **105**, 246803 (2010).

[6] A. Varykhalov, D. Marchenko, M. R. Scholz, E. Rienks, T. K. Kim, and O. Rader, arXiv:1104.3308.

[7] F. Libisch *et al.* , Phys. Rev. B, **81**, 245411 (2011).

[8] C. Busse *et al.*, Phys. Rev. Lett. **107**, 036101 (2011).

[9] A. T. N'Diyae *et al.*, New. J. Phys. **10**, 043033 (2008); Phys. Rev. Lett. **95**, 215501 (2006).